

# Geophysical Research Letters<sup>®</sup>

## RESEARCH LETTER

10.1029/2023GL107700

### Key Points:

- Direct measurement of P and S wave velocities of stishovite at mantle pressures and temperatures
- In the eclogite, coesite-stishovite transition can result in seismically detectable first order increase in P and S velocities
- An eclogite-rich layer model can interpret the seismic X-discontinuity in Hawaii area

### Supporting Information:

Supporting Information may be found in the online version of this article.

### Correspondence to:

S. Chen,  
[sibochen92@gmail.com](mailto:sibochen92@gmail.com)

### Citation:

Chen, S., Wang, S., Qi, X., Xu, M., Yu, T., Wang, Y., & Li, B. (2024). Sound velocities of stishovite at simultaneous high pressure and high temperature suggest an eclogite-rich layer beneath the Hawaii hotspot. *Geophysical Research Letters*, 51, e2023GL107700. <https://doi.org/10.1029/2023GL107700>

Received 6 DEC 2023  
Accepted 16 JUL 2024






### Author Contributions:

**Conceptualization:** Baosheng Li  
**Data curation:** Siheng Wang, Xintong Qi, Baosheng Li  
**Funding acquisition:** Baosheng Li  
**Investigation:** Siheng Wang, Xintong Qi, Man Xu, Tony Yu, Yanbin Wang  
**Software:** Baosheng Li  
**Supervision:** Baosheng Li  
**Writing – review & editing:** Siheng Wang, Xintong Qi, Man Xu, Tony Yu, Yanbin Wang, Baosheng Li

© 2024. The Author(s).

This is an open access article under the terms of the [Creative Commons Attribution-NonCommercial-NoDerivs License](https://creativecommons.org/licenses/by/4.0/), which permits use and distribution in any medium, provided the original work is properly cited, the use is non-commercial and no modifications or adaptations are made.

## Sound Velocities of Stishovite at Simultaneous High Pressure and High Temperature Suggest an Eclogite-Rich Layer Beneath the Hawaii Hotspot

Sibo Chen<sup>1,2</sup> , Siheng Wang<sup>1</sup> , Xintong Qi<sup>3</sup>, Man Xu<sup>4</sup> , Tony Yu<sup>4</sup> , Yanbin Wang<sup>4</sup>, and Baosheng Li<sup>1,3</sup> 

<sup>1</sup>Department of Geosciences, Stony Brook University, Stony Brook, NY, USA, <sup>2</sup>Now at School of Earth and Space Exploration, Arizona State University, Tempe, AZ, USA, <sup>3</sup>Mineral Physics Institute, Stony Brook University, Stony Brook, NY, USA, <sup>4</sup>Center for Advanced Radiation Sources, The University of Chicago, Chicago, IL, USA

**Abstract** Compressional and shear wave velocities of polycrystalline stishovite (SiO<sub>2</sub>) have been measured at simultaneous high pressures and temperatures up to 14.5 GPa and 800°C. By fitting velocities to the finite strain equations, the elastic moduli and density were determined to be  $K_{SO} = 306.6(46)$  GPa,  $K_S' = 4.92(10)$ ,  $\partial K_S'/\partial T = -0.024(1)$  GPa/K,  $G_0 = 229.0(34)$  GPa,  $G' = 1.07(10)$ ,  $\partial G/\partial T = -0.017(1)$  GPa/K,  $\rho_0 = 4.287(2)$  g/cm<sup>3</sup>. Our modeling suggested that, in the eclogite, coesite-stishovite transition can increase P and S wave velocities by 2.4% and 3.5%, respectively. A comparison between geophysical observations and our model shows that the coesite-stishovite phase transition in the eclogite can potentially be responsible for the occurrence of the X discontinuity beneath Hawaii. In addition, our current results suggest an eclogite-rich layer between 340 and 450 km depth beneath Hawaii. The eclogite concentration at the top and bottom of the layer is 41–55 vol% and >77 vol%, respectively.

**Plain Language Summary** In this study, we investigated the elastic behavior of stishovite, a high-pressure mineral found in subducted oceanic crust, under simultaneous high pressure and high temperature. By measuring compressional and shear wave velocities of polycrystalline stishovite at pressures up to 14.5 GPa and temperatures up to 800°C, we determined elastic modulus for stishovite. Using current data, we developed a model to predict seismic wave velocities changes in the subducted oceanic crust known as eclogite. According to our model, the coesite-stishovite phase transition can lead to a 2.4% and 3.5% increase in P and S wave velocities of eclogite, respectively. In addition, we compared it with geophysical observations, particularly focusing on the X discontinuity beneath Hawaii. Our result indicates the presence of an eclogite-rich layer beneath Hawaii, extending from 340 to 450 km in depth. The concentration of eclogite at the top and bottom of this layer varies, with values ranging from 41% to 55% at approximately 336 km and exceeding 77% at around 448 km depth.

## 1. Introduction

Stishovite is a high-pressure polymorph of silica (SiO<sub>2</sub>) and is stable above 9 GPa at 1,000°C, with a tetragonal structure (space group P4<sub>2</sub>/mnm). In silica-rich mineral assemblies, such as oceanic crust, stishovite is one of the major components at depth greater than ~300 km (Aoki & Takahashi, 2004; Ono, 1998). Previous experiment suggested that the velocity contrast between stishovite and coesite can be as high as ~45%, which might be responsible for the seismic X-discontinuities in the Earth's upper mantle (T. Chen et al., 2015, 2017).

The X-discontinuity at depths between 250 and 350 km has been observed by seismic studies in various geological settings such as subduction zones, stable continents, and hot-spots (Kemp et al., 2019; Pugh et al., 2021; Schmerr et al., 2013; Srinu et al., 2021; Wölbern & Rumpker, 2018). Using receiver functions analysis, Kemp et al. (2019) reported an X-discontinuity beneath the Hawaii hot-spot and interpreted this X-discontinuity as the coesite-stishovite phase transition.

Previous studies have reported the elastic properties of stishovite at room temperature and high pressure (Jiang et al., 2009; B. Li et al., 1996; Zhang et al., 2021). In Addition, using first-principles simulation with local density approximation, Yang and Wu (2014) calculated elastic constant tensor of stishovite at mantle pressure and temperature. However, elastic properties, especially the shear properties, of stishovite at simultaneous high pressure and temperature have not been directly constrained by experimental studies. In this study, we measured

the compressional and shear wave velocities of poly-crystalline stishovite at simultaneous high pressure and high temperature. Based on our data, we calculated the velocity profile of eclogite and discussed its possible role in interpreting the X-discontinuity in the Hawaii hot spot.

## 2. Experimental Methods

The polycrystal stishovite was synthesized from fused SiO<sub>2</sub> cylinder (3 mm in both diameter and thickness) from Goodfellow Corporation (purity >99.9%). The fused SiO<sub>2</sub> cylinder was enclosed in a gold capsule and hot-pressed at ~14 GPa and 1,200°C for 2 hr in the USCA-2000 multi-anvil apparatus installed at Stony Brook University. The recovered sample was characterized by scanning electron microscopy (Figure S1 in Supporting Information S1) and X-ray diffraction, which suggest that the grain size is less than 1 μm and the sample is a single phase of stishovite with no impurity phases present. By using the Archimedes' immersion method, the bulk density of the recovered stishovite sample was determined to be 4.269(10) g/cm<sup>3</sup>, which is 99.6% of the density [4.287(2) g/cm<sup>3</sup>] determined by the energy-dispersive X-ray diffraction (Figure S2 in Supporting Information S1).

Simultaneous high pressure and high temperature ultrasonic experiments were conducted in the 1,000-ton Kawaiii type (T-25) multi-anvil apparatus up to 14 GPa and 800°C in conjunction with synchrotron X-ray diffraction and imaging at GSECARS beamline 13-ID-D, Advanced Photon Source, Argonne National Laboratory. Figure S3 in Supporting Information S1 illustrates the cross section of the ultrasonic cell assembly. The apparatus compresses eight WC cubes, each with a corner truncated to the edge length of 8 mm, forming an octahedral cavity, within which a 14 mm MgO-MgAl<sub>2</sub>O<sub>4</sub> octahedral pressure transmitting medium was compressed. The high temperature was generated by a graphite heater and measured by a pair of W95Re5-W74Re26 thermocouple. A polycrystalline Si<sub>3</sub>N<sub>4</sub> cylinder (S. Wang et al., 2024) and a NaCl + BN (9: 1 by weight) disk were in contact with the front and rear surfaces of the sample to serve as the acoustic buffer rod and backing material marker, respectively. Two pieces of gold foils (2-μm thickness) were placed at the bottom and top of the sample, which served as X-ray image markers for the boundary of the sample and mechanical coupling material between the buffer rod and sample. The surfaces of the truncated corners of the WC cube, Si<sub>3</sub>N<sub>4</sub> buffer rod, and sample were all polished to 1 μm finish with diamond paste. Before the ultrasonic experiment, the length of the stishovite sample was measured with a micrometer, yielding a value of 1.536(1) mm.

By employing a dual mode LiNbO<sub>3</sub> transducer, P (50 MHz) and S (35 MHz) wave travel times were obtained simultaneously using a transfer function method (Li et al., 2005). Details of data acquisition and analysis can be found in B. Li and Liebermann (2014). Figure S4 in Supporting Information S1 shows the representative P and S wave signals at 12.1 GPa and 27°C, and the high signal-to-noise ratio echoes marked as “Anvil,” Buffer Rod” and “Sample” are reflections from the back surfaces of the WC cube, buffer rod and sample, respectively. During the ultrasonic experiment, the pressure was calculated directly using the experimental data of the sample (i.e., absolute pressure scale) (B. Li et al., 2005). At high pressure and temperature, the sample density and length were determined by X-ray diffraction and X-ray radiographic imaging technique, respectively (B. Li et al., 2004). Energy dispersive X-ray diffraction of the stishovite sample was collected at 2θ of 6.09°. The data was collected along cooling path in each heating-cooling cycle. The X-ray diffraction pattern was refined by the Le Bail method (e.g., Figure S5 in Supporting Information S1) in GSAS/EXPGUI (Larson & Von Dreele, 2000; Toby, 2001) to obtain the cell parameter and hence density. Figure S6 in Supporting Information S1 illustrates a representative X-radiographic image. The sample length was determined by measuring the pixel numbers between the two gold foils at the top and the bottom of the sample. Details of X-ray radiographic imaging technique can be found in B. Li et al. (2004). Using the two-layer bond correction model (Noda et al., 2022), the P and S wave travel time were corrected by 3.46 and 4.03 ns, respectively.

## 3. Results and Discussion

After the high pressure ultrasonic experiment, the length of the recovered sample measured by micrometer yield 1.536(1) mm, which is identical to its original length before the experiment. This indicates that the sample was under near-hydrostatic pressure conditions, and no plastic deformation had occurred within the sample.

P and S wave velocities of poly-crystalline stishovite versus pressure were plotted and listed in Figure 1 and Table S1 in Supporting Information S1, respectively. Within the current experimental P-T range, the P and S wave velocities monotonically increased with pressure and decreased with temperature. At room temperature (27°C),

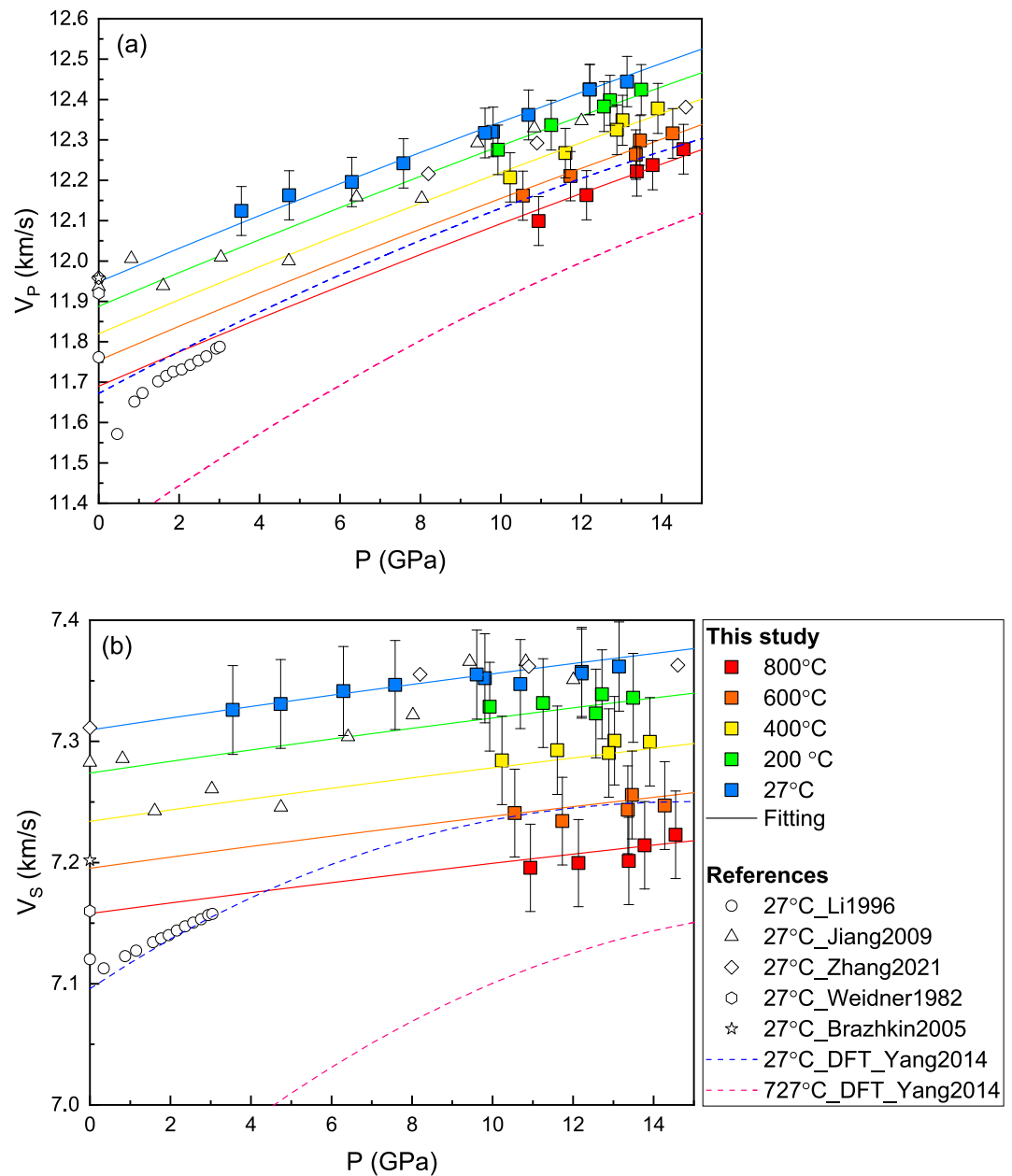


**Figure 1.** (a) Compressional and (b) shear wave velocities of stishovite. Color squares: ultrasonic data in this study; color lines: finite strain equations fitting; empty circles: previous ultrasonic data (B. Li et al., 1996); empty triangles, diamond, star and hexagon: VRH average of previous Brillouin scattering data (Brazhkin et al., 2005; Jiang et al., 2009; Weidner et al., 1982; Zhang et al., 2021); Color dash lines: DFT simulation data (Yang & Wu, 2014).

both P and S wave velocities agree with previous single-crystal Voigt-Reuss-Hill (VRH) average values within  $\sim 1\%$  of Jiang et al. (2009) and Zhang et al. (2021) and up to 2.1% higher than those from Weidner et al. (1982) and Brazhkin et al. (2005). In addition, the  $V_P$  and  $V_S$  obtained in this study are  $\sim 1.5\text{--}2.7\%$  higher than previous ultrasonic measurements (B. Li et al., 1996), which may be due to the presence of pores and/or impurity phase in the previous study.

Combining the sound velocities with the density determined by X-ray diffraction, the bulk and shear moduli were derived using  $K_S = \rho V_P^2 - 4 \rho V_S^2/3$  and  $G = \rho V_S^2$ , respectively. Figure S7 in Supporting Information S1 illustrated the elastic moduli versus pressure. Within the 14.5 GPa pressure range, the adiabatic bulk and shear

**Table 1**

Comparison of Elastic Moduli of Stishovite With Previous Experimental and Calculation Results (Andrault et al., 2003; Brazhkin et al., 2005; Jiang et al., 2009; Karki et al., 1997; B. Li et al., 1996; J. Liu et al., 1999; Luo et al., 2002; Nishihara et al., 2005; F. Wang et al., 2012; Weidner et al., 1982; Yamanaka et al., 2002; Yang & Wu, 2014; Zhang et al., 2021)

Method	$K_{S0}$ (GPa)	$K_S'$	$\partial K_S/\partial T$ GPa/K	$K_{T0}$ (GPa)	$K_T'$	$\partial K_T/\partial T$ (GPa/K)	$G_0$ (GPa)	$G'$	$\partial G/\partial T$ (GPa/K)	$P_{\max}$ (GPa)	$T_{\max}$ (°C)	Reference
Ultrasound	<b>306.6 (46)</b>	<b>4.92 (10)</b>	<b>-0.024 (1)</b>	<b>308.2(46)<sup>a</sup></b>	<b>4.90(10)<sup>b</sup></b>	<b>-0.031<sup>c</sup></b>	<b>229.0 (34)</b>	<b>1.07 (10)</b>	<b>-0.017 (1)</b>	<b>14.5</b>	<b>800</b>	<b>This study</b>
	305(5)	5.3(1)					217(4)	1.8(1)		3	Ambient	Li et al. (1996)
Brillouin scattering	308(1)	4(1)					228(1)	1.1(1)		12	Ambient	Jiang et al. (2009)
	307.5	4					229.4	1		Re-fit to 14.6	Ambient	Zhang et al. (2021)
	316(4)						220(3)			Ambient	Ambient	Weidner et al. (1982)
	316(4)						222(5)			Ambient	Ambient	Brazhkin et al. (2005)
Theoretical calculation	290.1	5.02	-0.027				213.1	1.71	-0.018	Re-fit to 15.0	Re-fit to 727	Yang and Wu (2014)
	312						226			Ambient	-273	Karki et al. (1997)
Shock wave				306(5)	5.0(2)					250	corrected to ambient	Luo et al. (2002)
XRD				297(5)	4.3(4)	-0.046 (5)				22	800	Nishihara et al. (2005)
	296(2)			294(2)	4.85(12)					54	1,427	Wang et al. (2012)
				294(2)	5.3 (fixed)	-0.041 (11)				10	1,000	Liu et al. (1999)
				309.9(11)	4.59(23)					53	Ambient	Andrault et al. (2003)
			292(13)	6 (fixed)					29.1	Ambient	Yamanaka et al. (2002)	

Note. Where  $\alpha$  is thermal expansion coefficient,  $\gamma$  is Grüneisen parameter.  ${}^a K_{T0} = K_S/(1 + \alpha\gamma T)$ .  ${}^b K_T' = [K_S' - \gamma T/K_T (\partial K_T/\partial T)]/(1 + \alpha\gamma T)$ .  ${}^c \partial K_T/\partial T = (\partial K_S/\partial T)/(1 + \alpha\gamma T) - K_S/(1 + \alpha\gamma T)^2 [\alpha\gamma + (\partial\alpha/\partial T)\gamma T]$ .

moduli increase with increasing pressure. Together with thermal expansion coefficient  $\alpha_a = 1.26 \cdot 10^{-5} \text{K}^{-1}$ ,  $\alpha_b = 1.29 \cdot 10^{-8} \text{K}^{-2}$  (Nishihara et al., 2005) and Grüneisen parameter  $\gamma = 1.34$  (Stixrude & Lithgow-Berteloni, 2005), the current data was fitted to the third-order Eulerian finite strain equations (Davies & Dziewonski, 1975; B. Li and Zhang, 2005; S. Wang et al., 2021), the elastic bulk and shear moduli and their pressure and temperature derivatives were calculated, yielding  $K_{S0} = 306.6(46)$  GPa,  $K_S' = 4.92(10)$ ,  $\partial K_S/\partial T = -0.024(1)$  GPa/K,  $G_0 = 229.0(34)$  GPa,  $G' = 1.07(10)$ , and  $\partial G/\partial T = -0.017(1)$  GPa/K.

Table 1 compared the current result with previous sound velocity and equation of state studies. Using Brillouin scattering, Weidner et al. (1982) reported the  $K_{S0}$  and  $G_0$  of 316 and 220 GPa, respectively. Brazhkin et al. (2005) confirmed this observation with the  $K_{S0}$  and  $G_0$  of 316 and 222 GPa, respectively. Jiang et al. (2009) measured the elasticity of single crystal stishovite up to 12 GPa at ambient temperature, the  $K_{S0}$  and  $G_0$  of poly-crystal stishovite were derived as 308 and 228 GPa, respectively. A later study (Zhang et al., 2021) measured the elastic moduli of single crystal stishovite/post-stishovite at 0–70 GPa using Brillouin scattering and impulsive stimulated light scattering. By re-fitting the data (up to 14.6 GPa) to the finite strain equations, the  $K_0$  and  $G_0$  of poly-crystal stishovite yield 307.5 and 229.4 GPa. The current bulk moduli (306.6 GPa) and shear moduli (229.0 GPa) are in good agreement with the previous high pressure Brillouin studies. Using density functional theory (DFT) simulation, Yang and Wu (2014) calculated the elastic moduli of stishovite up to 65 GPa and 2,727°C. By re-fitting the data up to 15 GPa and 727°C, the temperature derivatives of the bulk and shear moduli are -0.027 and -0.018 GPa/K, respectively, which agree well with our current study. The  $V_P$  and  $V_S$  at ambient conditions, calculated from  $K_{S0}$  and  $G_0$  in this study, are 11.948(60) and 7.309(37) km/s, respectively. Those values are consistent with those reported by Brillouin scattering studies within 0.5%.

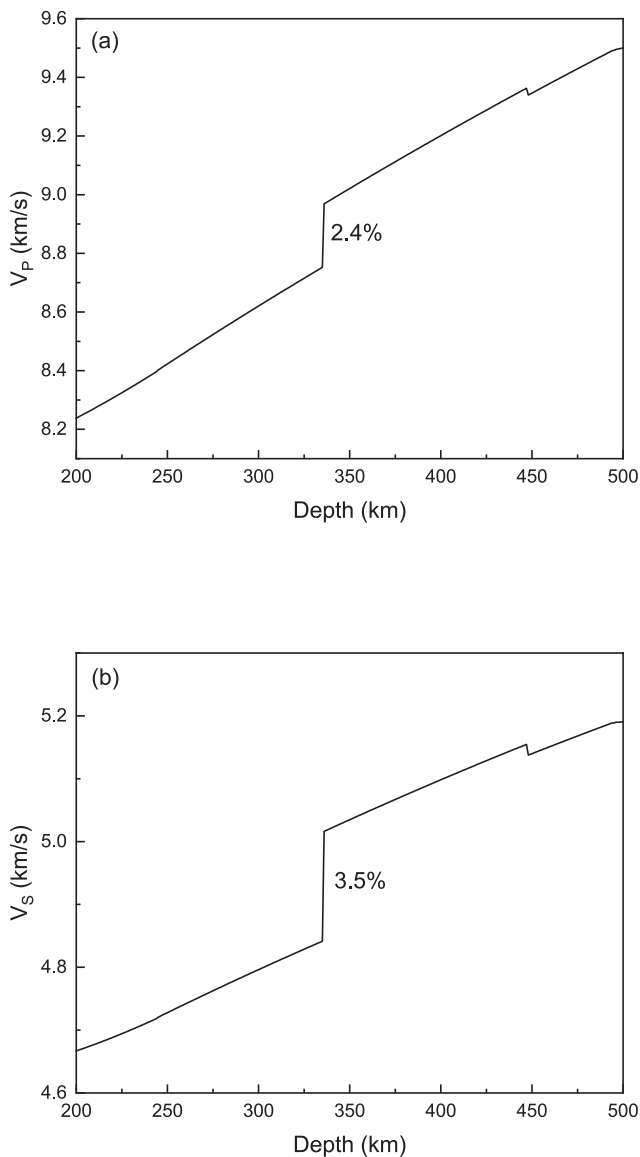


**Figure 2.** (a) Compressional (P), and (b) shear (S) velocities of eclogite along adiabat temperature + 170°C.

indicated the coesite-stishovite transition in an eclogite + harzburgite layer can potentially explain the X-discontinuity in Hawaii area. To explore this hypothesis further, we calculated velocity profiles beneath the Hawaii hotspot.

The preliminary reference Earth model (Dziewonski & Anderson, 1981) suggested, at depth of 336 km, the pressure is about 11.1 GPa corresponding to a temperature of 1,637°C according to the coesite-stishovite phase boundary (Akaogi et al., 2011). Notably, this temperature is 170°C higher than the temperature along a recently proposed 1,373°C (1646 K) adiabat geotherm (Katsura, 2022) at depth of 336 km. By analyzing olivine-liquid equilibria and olivine phenocrysts, Putirka (2005) suggested that the mean temperature in Hawaii is 1,620(55)°C and the derived potential temperature is 213–235°C higher than that of ambient middle ocean ridges. In addition, a seismic study indicated that temperature of the mantle beneath Hawaii is 87–129°C higher than ambient mantle conditions (Courtier et al., 2007). A more recent seismic study (Bao et al., 2022) confirmed this observation with an even higher excess temperature range (121–206°C). The estimated temperature (1,637°C) is in general agreement with the temperature range given above. Therefore, we calculated the P and S wave velocities of coesite (T. Chen et al., 2015, 2017) and stishovite along the adiabat temperature profile

To compare with previous equation of state studies, we converted the adiabatic bulk moduli and its pressure and temperature derivatives to isothermal values using equations in Speziale and Duffy (2002). The calculated  $K_{T0}$  (308.2 GPa) and  $K_T'$  (4.90) are within the range ( $K_{T0}$ : 292–309.9 GPa,  $K_T'$ : 4.3–6) reported in previous studies (Andrault et al., 2003; J. Liu et al., 1999; Luo et al., 2002; Nishihara et al., 2005; F. Wang et al., 2012; Yamanaka et al., 2002). The  $\partial K_T/\partial T$  (–0.031 GPa/K) calculated from  $\partial K_S/\partial T$  is ~0.01 GPa/K higher than that determined by X-ray diffraction studies (J. Liu et al., 1999; Nishihara et al., 2005), which could be in part caused by the tradeoff between the bulk modulus and its pressure and/or temperature derivative during equation of state data analyses in different studies.

#### 4. Implication for Detecting Eclogite in the Hawaii Hotspot

Kemp et al. (2019) identified an X-discontinuity beneath the Hawaii hot-spot through receiver function analysis. Their findings indicate that to the east of the Big Island, the X-discontinuity is located at a depth of approximately 336 km, displaying a strong receiver function amplitude. In contrast, the “410” discontinuity was observed at a depth of 446 km, exhibiting an extremely weak amplitude. Previous studies used the formation of phase A (L.-G. Liu, 1987; Revenaugh & Jordan, 1991) [forsterite + H<sub>2</sub>O → enstatite + phase A] to explain the X-discontinuity in the upper mantle. However, this reaction requires low temperature (up to 1,000°C at 300 km) and high water concentration in the mantle (Komabayashi et al., 2005). Such conditions cannot be met in the hot environment in the Hawaii area. A later study, which conducted experiments up to 1,600°C and suggested that formation of anhydrous phase B (forsterite + periclase → anhydrous phase B) can potentially contribute to the X-discontinuity (Ganguly & Frost, 2006). However, this reaction requires free ferropericlase to occur in subduction zones (Ganguly & Frost, 2006). Another proposed mechanism is the orthopyroxene-high pressure clinopyroxene phase transition (Angel et al., 1992; Woodland, 1998). However, more recent studies suggest that this phase transition can only produce weak impedance contrast in mantle peridotite (T. Chen et al., 2015; Schmerr, 2015; Xu et al., 2008), especially at higher temperature, hence may not be seismically detectable. Another possible candidate for the X-discontinuity is coesite-stishovite phase transition (T. Chen et al., 2015, 2017; Schmerr, 2015; Williams & Revenaugh, 2005). Using dynamic simulation, Ballmer et al. (2013) explored a eclogite-rich plume. Their results suggested that a silica-bearing eclogite-rich layer can be formed at depth around 300 – 410 km. Kemp et al. (2019)

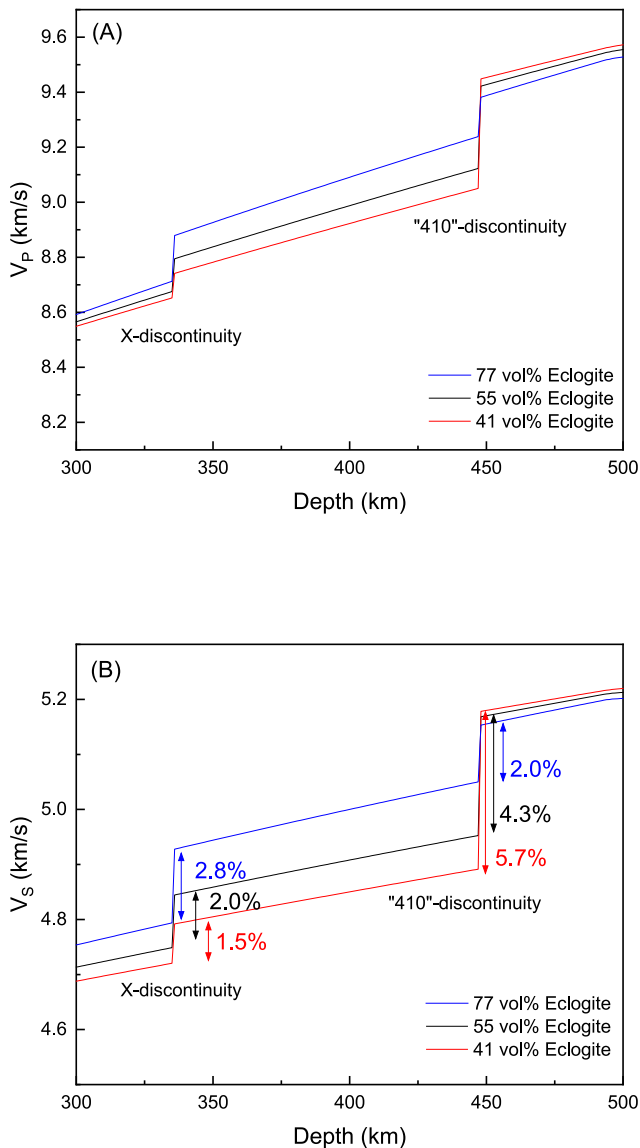


**Figure 3.** (a) Compressional and (b) shear wave velocities of eclogite + harzburgite, assuming minerals are mechanically mixed.

(Katsura, 2022) +170°C. The result is shown in Figure S8 in Supporting Information S1. At 336 km depth, the  $V_P$  and  $V_S$  contrast (defined as  $\frac{V_{stiv} - V_{coe}}{0.5(V_{stiv} + V_{coe})}$ ) between the coesite and stishovite is 39% and 56%, respectively. Following the same P-T profile, together with the elastic data of garnet and clinopyroxene (Gwanmesia et al., 2014; Hao et al., 2019, 2021), we further calculated the one-dimensional velocity-depth profiles of eclogite by using Voigt-Reuss-Hill averages (S. Chen et al., 2022; Hill, 1963). The mineral proportion was referred to Aoki and Takahashi (2004) (Figure S9a in Supporting Information S1). The results (Figure 2) suggest that at 336 km, even with 5.6 vol% free silica (Aoki & Takahashi, 2004), the coesite-stishovite phase transition can produce  $V_P$  and  $V_S$  contrast by 2.4% and 3.5%, respectively. A broadband array observations suggested the  $V_S$  contrast of X-discontinuity at Hawaii is 1.5%–2% (Schmerr et al., 2013). Based on previous elastic data (Gwanmesia et al., 2006; Kung et al., 2005; W. Liu et al., 2005, 2009) and mineralogical model of harzburgite (Figure S9b in Supporting Information S1) (Irifune & Ringwood, 1987), we calculated the velocities for an aggregate with eclogite + harzburgite composition assuming that they are mechanically mixed. The result was plotted in Figure 3. The calculated profile suggests that an aggregate with 41%–55 vol% eclogite can produce 1.5%–2%  $V_S$  contrast at depth of 336 km. This result is in good agreement with that estimated using synthetic receiver function amplitude (e.g., 40%–50% eclogite + 50%–60% harzburgite) (Kemp et al., 2019). With depth increased to 448 km, due to the olivine-wadsleyite phase transition in the harzburgite, the  $V_S$  further increases and the contrast is 4.3%–5.7%, which is up to ~4 times higher than that of the X-discontinuity at 336 km. This high  $V_S$  contrast results in the higher amplitude of the “410” discontinuity. However, the seismic observations suggested that, in the Hawaii area, the amplitude of the X-discontinuity is stronger than that of the “410” discontinuity (Kemp et al., 2019). This discrepancy could be indicative of a higher eclogite content (e.g., >77 vol%) at depth of 448 km.

Our calculation result tends to support the eclogite-rich layer model in the Hawaii area (Figure 4). At the top of the layer the eclogite concentration is 41%–55%, while the value increased to >77% at the bottom. However, the remaining question is where eclogite comes from. Previous dynamic simulations suggest that the recycled oceanic crust can be entrained by the mantle plume and brought back to the upper mantle (M. Li, 2021). Ballmer et al. (2013) performed a regional modeling at Hawaii, and their result showed that the thermochemical plumes containing an eclogite component tended to form a layer at ~300–410 km depth. Dannberg and Sobolev (2015) also showed that under certain temperature and plume size, the thermochemical plumes can entrain recycled oceanic crust. In addition to that, previous seismic study reported a mid-mantle discontinuity at ~1,050 km depth beneath Hawaii (Shen et al., 2003), which can possibly be interpreted by the stishovite–post-stishovite phase transition (Yang & Wu, 2014; Zhang et al., 2021, 2022). This further supports the existence of recycled crust in the lower mantle, if assuming the free silica was from the recycled crust. Hence, the eclogite can be possibly transported by the mantle plume from lower mantle to the upper mantle. Once the plume rises through the olivine-wadsleyite phase transition, it becomes less buoyant and begins to accumulate and spread out, ultimately forming an eclogite-rich layer (Ballmer et al., 2013). At the top of the layer (~336 km) the eclogite concentration is 41%–55 vol%. Due to the coesite-stishovite phase transition, the S-wave velocity of the bulk assembly increased by 1.5%–2% and was detected as the X-discontinuity. At the bottom of the layer (~448 km), the eclogite concentration increased to >77 vol%, consequently diminishing the amplitude of the “410” discontinuity.

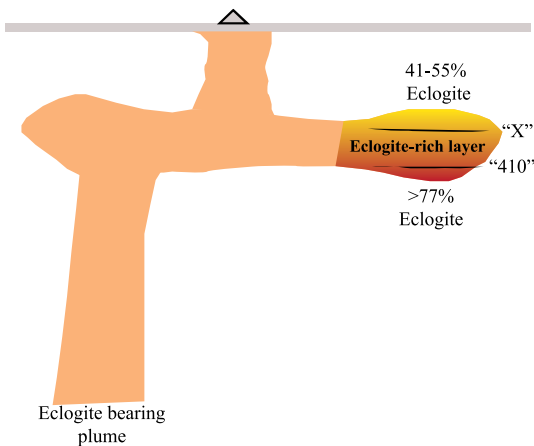


**Figure 4.** Schematic illustration of the deep eclogite-rich layer in the Hawaii area (modified from Kemp et al., 2019).

## 5. Conclusions

We investigated the compressional and shear velocities of polycrystalline stishovite up to 14.5 GPa and 800°C using ultrasonic interferometry with in situ synchrotron X-rays. Within the P-T range, the P and S velocities, as well as the adiabatic bulk and shear moduli, exhibit a monotonic increase with increasing pressure and decrease with increasing temperature. By fitting the measured velocities to the third-order Eulerian finite strain equations, the elastic moduli of stishovite and their pressure and temperature derivatives were obtained, yielding  $K_{S0} = 306.6(46)$  GPa,  $K_S' = 4.92(10)$ ,  $\partial K_S/\partial T = -0.024(1)$  GPa/K,  $G_0 = 229.0(34)$  GPa,  $G' = 1.07(10)$ , and  $\partial G/\partial T = -0.017(1)$  GPa/K. With the current data together with those from literature for other mantle phases, we calculated the velocity profile of the eclogite in the Hawaii area, and found that at 336 km depth the P and S wave velocities of the eclogite exhibit first order increases with a velocity contrast of 2.4% and 3.5%, respectively. A comparison between receiver function observation in Hawaii and the velocity contrasts of eclogite + harzburgite shows that the coesite-stishovite transition in the eclogite can potentially be

responsible for the occurrence of the X discontinuity. Our results tend to support the eclogite-rich model in Hawaii. The eclogite concentration at the top (~336 km) and bottom (~448 km) of the layer is 41–55 vol.% and >77 vol.% respectively.

## Data Availability Statement

The original data collected by this study can be found in Zenodo (S. Chen, 2024). The elastic data of mantle minerals are available in Gwanmesia et al. (2014, 2006), Hao et al. (2021, 2019), Kung et al. (2005), W. Liu et al. (2005, 2009), and T. Chen et al. (2015, 2017). The mineral proportions data are available in Akaogi et al. (2011) and Irifune and Ringwood (1987).

## References

- Akaogi, M., Oohata, M., Kojitani, H., & Kawaji, H. (2011). Thermodynamic properties of stishovite by low-temperature heat capacity measurements and the coesite-stishovite transition boundary. *American Mineralogist*, *96*(8–9), 1325–1330. <https://doi.org/10.2138/am.2011.3748>
- Andraut, D., Angel, R. J., Mosenfelder, J. L., & Le Bihan, T. (2003). Equation of state of stishovite to lower mantle pressures. *American Mineralogist*, *88*(2–3), 301–307. <https://doi.org/10.2138/am-2003-2-307>
- Angel, R. J., Chopelas, A., & Ross, N. (1992). Stability of high-density clinoenstatite at upper-mantle pressures. *Nature*, *358*(6384), 322–324. <https://doi.org/10.1038/358322a0>
- Aoki, I., & Takahashi, E. (2004). Density of MORB eclogite in the upper mantle. *Physics of the Earth and Planetary Interiors*, *143*, 129–143. <https://doi.org/10.1016/j.pepi.2003.10.007>
- Ballmer, M. D., Ito, G., Wolfe, C. J., & Solomon, S. C. (2013). Double layering of a thermochemical plume in the upper mantle beneath Hawaii. *Earth and Planetary Science Letters*, *376*, 155–164. <https://doi.org/10.1016/j.epsl.2013.06.022>
- Bao, X., Lithgow-Bertelloni, C. R., Jackson, M. G., & Romanowicz, B. (2022). On the relative temperatures of Earth's volcanic hotspots and mid-ocean ridges. *Science*, *375*(6576), 57–61. <https://doi.org/10.1126/science.abj8944>
- Brazhkin, V., McNeil, L., Grimsditch, M., Bendeliani, N., Dyuzheva, T., & Lityagina, L. (2005). Elastic constants of stishovite up to its amorphization temperature. *Journal of Physics: Condensed Matter*, *17*(12), 1869–1875. <https://doi.org/10.1088/0953-8984/17/12/011>
- Chen, S. (2024). Sound velocities of stishovite at simultaneous high pressure and high temperature suggest an eclogite-rich layer beneath the Hawaii hotspot [Dataset]. *Zenodo*. <https://doi.org/10.5281/zenodo.12173805>
- Chen, S., Cai, N., Wang, S., Qi, X., & Li, B. (2022). Implications of sound velocities of natural topaz on the seismic L-discontinuity. *Geophysical Research Letters*, *49*(2), e2021GL095107. <https://doi.org/10.1029/2021gl095107>
- Chen, T., Gwanmesia, G. D., Wang, X., Zou, Y., Liebermann, R. C., Michaut, C., & Li, B. (2015). Anomalous elastic properties of coesite at high pressure and implications for the upper mantle X-discontinuity. *Earth and Planetary Science Letters*, *412*, 42–51. <https://doi.org/10.1016/j.epsl.2014.12.025>
- Chen, T., Liebermann, R. C., Zou, Y., Li, Y., Qi, X., & Li, B. (2017). Tracking silica in Earth's upper mantle using new sound velocity data for coesite to 5.8 GPa and 1073 K. *Geophysical Research Letters*, *44*(15), 7757–7765. <https://doi.org/10.1002/2017gl073950>
- Courtier, A. M., Bagley, B., & Revenaugh, J. (2007). Whole mantle discontinuity structure beneath Hawaii. *Geophysical Research Letters*, *34*(17), L17304. <https://doi.org/10.1029/2007gl031006>
- Dannberg, J., & Sobolev, S. V. (2015). Low-buoyancy thermochemical plumes resolve controversy of classical mantle plume concept. *Nature Communications*, *6*(1), 1–9. <https://doi.org/10.1038/ncomms7960>
- Davies, G. F., & Dziewonski, A. M. (1975). Homogeneity and constitution of the earth's lower mantle and outer core. *Physics of the Earth and Planetary Interiors*, *10*(4), 336–343. [https://doi.org/10.1016/0031-9201\(75\)90060-6](https://doi.org/10.1016/0031-9201(75)90060-6)
- Dziewonski, A. M., & Anderson, D. L. (1981). Preliminary reference Earth model. *Physics of the Earth and Planetary Interiors*, *25*(4), 297–356. [https://doi.org/10.1016/0031-9201\(81\)90046-7](https://doi.org/10.1016/0031-9201(81)90046-7)

## Acknowledgments

We would like to thank Robert Liebermann for language editing. This work is supported by grants to BL from DOE/NNSA (DE-NA0004085). Use of the COMPRES Cell Assembly Project was supported by COMPRES under NSF Cooperative Agreement (EAR-1661511). The ultrasonic measurements were performed at GeoSoilEnviroCARS beamline 13-ID-D, Advanced Photon Source (APS), Argonne National Laboratory. GSECARS is supported by the NSF-Earth Sciences (EAR-1634415) and Department of Energy-GeoSciences (DE-FG02-94ER14466). This research used resources of the Advanced Photon Source, a U.S. Department of Energy (DOE) Office of Science User Facility operated for the DOE Office of Science by Argonne National Laboratory under Contract DE-AC02-06CH11357.

- Ganguly, J., & Frost, D. J. (2006). Stability of anhydrous phase B: Experimental studies and implications for phase relations in subducting slab and the X discontinuity in the mantle. *Journal of Geophysical Research*, *111*(B6). <https://doi.org/10.1029/2005jb003910>
- Gwanmesia, G. D., Wang, L., Heady, A., & Liebermann, R. C. (2014). Elasticity and sound velocities of polycrystalline grossular garnet ( $\text{Ca}_3\text{Al}_2\text{Si}_3\text{O}_{12}$ ) at simultaneous high pressures and high temperatures. *Physics of the Earth and Planetary Interiors*, *228*, 80–87. <https://doi.org/10.1016/j.pepi.2013.09.010>
- Gwanmesia, G. D., Zhang, J., Darling, K., Kung, J., Li, B., Wang, L., et al. (2006). Elasticity of polycrystalline pyrope ( $\text{Mg}_3\text{Al}_2\text{Si}_3\text{O}_{12}$ ) to 9 GPa and 1000 C. *Physics of the Earth and Planetary Interiors*, *155*(3–4), 179–190. <https://doi.org/10.1016/j.pepi.2005.10.008>
- Hao, M., Zhang, J. S., Pierotti, C. E., Ren, Z., & Zhang, D. (2019). High-pressure single-crystal elasticity and thermal equation of state of omphacite and their implications for the seismic properties of eclogite in the Earth's interior. *Journal of Geophysical Research: Solid Earth*, *124*(3), 2368–2377. <https://doi.org/10.1029/2018jb016964>
- Hao, M., Zhang, J. S., Zhou, W. Y., & Wang, Q. (2021). Seismic visibility of eclogite in the Earth's upper mantle—Implications from high pressure-temperature single-crystal elastic properties of omphacite. *Journal of Geophysical Research: Solid Earth*, *126*(5), e2021JB021683. <https://doi.org/10.1029/2021jb021683>
- Hill, R. (1963). Elastic properties of reinforced solids: Some theoretical principles. *Journal of the Mechanics and Physics of Solids*, *11*(5), 357–372. [https://doi.org/10.1016/0022-5096\(63\)90036-x](https://doi.org/10.1016/0022-5096(63)90036-x)
- Irfune, T., & Ringwood, A. (1987). Phase transformations in a harzburgite composition to 26 GPa: Implications for dynamical behaviour of the subducting slab. *Earth and Planetary Science Letters*, *86*(2–4), 365–376. [https://doi.org/10.1016/0012-821x\(87\)90233-0](https://doi.org/10.1016/0012-821x(87)90233-0)
- Jiang, F., Gwanmesia, G. D., Dyuzheva, T. I., & Duffy, T. S. (2009). Elasticity of stishovite and acoustic mode softening under high pressure by Brillouin scattering. *Physics of the Earth and Planetary Interiors*, *172*(3–4), 235–240. <https://doi.org/10.1016/j.pepi.2008.09.017>
- Karki, B. B., Stixrude, L., & Crain, J. (1997). Ab initio elasticity of three high-pressure polymorphs of silica. *Geophysical Research Letters*, *24*(24), 3269–3272. <https://doi.org/10.1029/97gl53196>
- Katsura, T. (2022). A revised adiabatic temperature profile for the mantle. *Journal of Geophysical Research: Solid Earth*, *127*(2), e2021JB023562. <https://doi.org/10.1029/2021jb023562>
- Kemp, M., Jenkins, J., Maclennan, J., & Cottaar, S. (2019). X-discontinuity and transition zone structure beneath Hawaii suggests a heterogeneous plume. *Earth and Planetary Science Letters*, *527*, 115781. <https://doi.org/10.1016/j.epsl.2019.115781>
- Komabayashi, T., Hirose, K., Funakoshi, K.-I., & Takafuji, N. (2005). Stability of phase A in antigorite (serpentine) composition determined by in situ X-ray pressure observations. *Physics of the Earth and Planetary Interiors*, *151*(3–4), 276–289. <https://doi.org/10.1016/j.pepi.2005.04.002>
- Kung, J., Li, B., Uchida, T., & Wang, Y. (2005). In-situ elasticity measurement for the unquenchable high-pressure clinopyroxene phase: Implication for the upper mantle. *Geophysical Research Letters*, *32*(1), L01307. <https://doi.org/10.1029/2004gl021661>
- Larson, A. C., & Von Dreele, R. B. (2000). *General structure analysis system (GSAS)Rep* (pp. 86–748). Los Alamos National Laboratory.
- Li, B., Kung, J., & Liebermann, R. C. (2004). Modern techniques in measuring elasticity of Earth materials at high pressure and high temperature using ultrasonic interferometry in conjunction with synchrotron X-radiation in multi-anvil apparatus. *Physics of the Earth and Planetary Interiors*, *143*, 559–574. <https://doi.org/10.1016/j.pepi.2003.09.020>
- Li, B., Kung, J., Uchida, T., & Wang, Y. (2005). Pressure calibration to 20 GPa by simultaneous use of ultrasonic and X-ray techniques. *Journal of Applied Physics*, *98*(1), 013521. <https://doi.org/10.1063/1.1946905>
- Li, B., & Liebermann, R. C. (2014). Study of the Earth's interior using measurements of sound velocities in minerals by ultrasonic interferometry. *Physics of the Earth and Planetary Interiors*, *233*, 135–153. <https://doi.org/10.1016/j.pepi.2014.05.006>
- Li, B., Rigden, S. M., & Liebermann, R. C. (1996). Elasticity of stishovite at high pressure. *Physics of the Earth and Planetary Interiors*, *96*(2–3), 113–127. [https://doi.org/10.1016/0031-9201\(96\)03144-5](https://doi.org/10.1016/0031-9201(96)03144-5)
- Li, B., & Zhang, J. Z. (2005). Pressure and temperature dependence of elastic wave velocity of  $\text{MgSiO}_3$  perovskite and the composition of the lower. *Physics of the Earth and Planetary Interiors*, *151*(1–2), 143–154. <https://doi.org/10.1016/j.pepi.2005.02.004>
- Li, M. (2021). The cycling of subducted oceanic crust in the Earth's deep mantle. *Mantle Convection and Surface Expressions*, 303–328. <https://doi.org/10.1002/9781119528609.ch12>
- Liu, J., Zhang, J., Flesch, L., Li, B., Weidner, D. J., & Liebermann, R. C. (1999). Thermal equation of state of stishovite. *Physics of the Earth and Planetary Interiors*, *112*(3–4), 257–266. [https://doi.org/10.1016/s0031-9201\(99\)00037-0](https://doi.org/10.1016/s0031-9201(99)00037-0)
- Liu, L.-G. (1987). Effects of  $\text{H}_2\text{O}$  on the phase behaviour of the forsterite-enstatite system at high pressures and temperatures and implications for the Earth. *Physics of the Earth and Planetary Interiors*, *49*(1–2), 142–167. [https://doi.org/10.1016/0031-9201\(87\)90138-5](https://doi.org/10.1016/0031-9201(87)90138-5)
- Liu, W., Kung, J., & Li, B. (2005). Elasticity of San Carlos olivine to 8 GPa and 1073 K. *Geophysical Research Letters*, *32*(16), L16301. <https://doi.org/10.1029/2005gl023453>
- Liu, W., Kung, J., Li, B., Nishiyama, N., & Wang, Y. (2009). Elasticity of ( $\text{Mg}_{0.87}\text{Fe}_{0.13}$ ) $2\text{SiO}_4$  wadsleyite to 12 GPa and 1073 K. *Physics of the Earth and Planetary Interiors*, *174*(1–4), 98–104. <https://doi.org/10.1016/j.pepi.2008.10.020>
- Luo, S. N., Mosenfelder, J., Asimow, P. D., & Ahrens, T. J. (2002). Direct shock wave loading of Stishovite to 235 GPa: Implications for perovskite stability relative to an oxide assemblage at lower mantle conditions. *Geophysical Research Letters*, *29*(14), 36. <https://doi.org/10.1029/2002gl015627>
- Nishihara, Y., Nakayama, K., Takahashi, E., Iguchi, T., & Funakoshi, K.-I. (2005). P-V-T equation of state of stishovite to the mantle transition zone conditions. *Physics and Chemistry of Minerals*, *31*(10), 660–670. <https://doi.org/10.1007/s00269-004-0426-7>
- Noda, M., Inoue, T., Tsuchiya, T., & Higo, Y. (2022). Reassessment of a bond correction method for in situ ultrasonic interferometry on elastic wave velocity measurement under high pressure and high temperature. *High Pressure Research*, *42*(3), 1–16. <https://doi.org/10.1080/08957959.2022.2112677>
- Ono, S. (1998). Stability limits of hydrous minerals in sediment and mid-ocean ridge basalt compositions: Implications for water transport in subduction zones. *J Geophys ResSolid Earth*, *103*(B8), 18253–18267. <https://doi.org/10.1029/98jb01351>
- Pugh, S., Jenkins, J., Boyce, A., & Cottaar, S. (2021). Global receiver function observations of the X-discontinuity reveal recycled basalt beneath hotspots. *Earth and Planetary Science Letters*, *561*, 116813. <https://doi.org/10.1016/j.epsl.2021.116813>
- Putirka, K. D. (2005). Mantle potential temperatures at Hawaii, Iceland, and the mid-ocean ridge system, as inferred from olivine phenocrysts: Evidence for thermally driven mantle plumes. *Geochemistry, Geophysics, Geosystems*, *6*(5). <https://doi.org/10.1029/2005gc000915>
- Revenaugh, J., & Jordan, T. H. (1991). Mantle layering from ScS reverberations: 3. The upper mantle. *Journal of Geophysical Research*, *96*(B12), 19781–19810. <https://doi.org/10.1029/91jb01487>
- Schmerr, N. C. (2015). Imaging mantle heterogeneity with upper mantle seismic discontinuities. In *The Earth's heterogeneous mantle* (pp. 79–104). Springer.
- Schmerr, N. C., Kelly, B. M., & Thorne, M. S. (2013). Broadband array observations of the 300 km seismic discontinuity. *Geophysical Research Letters*, *40*(5), 841–846. <https://doi.org/10.1002/grl.50257>



- Shen, Y., Wolfe, C. J., & Solomon, S. C. (2003). Seismological evidence for a mid-mantle discontinuity beneath Hawaii and Iceland. *Earth and Planetary Science Letters*, 214(1–2), 143–151. [https://doi.org/10.1016/s0012-821x\(03\)00349-2](https://doi.org/10.1016/s0012-821x(03)00349-2)
- Speziale, S., & Duffy, T. S. (2002). Single-crystal elastic constants of fluorite (CaF<sub>2</sub>) to 9.3 GPa. *Physics and Chemistry of Minerals*, 29(7), 465–472. <https://doi.org/10.1007/s00269-002-0250-x>
- Srinu, U., Kumar, P., Haldar, C., Kumar, M. R., Srinagesh, D., & Illa, B. (2021). X-Discontinuity beneath the Indian Shield—Evidence for remnant tethyan oceanic lithosphere in the mantle. *Journal of Geophysical Research: Solid Earth*, 126(8), e2021JB021890. <https://doi.org/10.1029/2021jb021890>
- Stixrude, L., & Lithgow-Bertelloni, C. (2005). Thermodynamics of mantle minerals—I. Physical properties. *Geophysical Journal International*, 162(2), 610–632. <https://doi.org/10.1111/j.1365-246x.2005.02642.x>
- Toby, B. H. (2001). EXPGUI, a graphical user interface for GSAS. *Journal of Applied Crystallography*, 34(2), 210–213. <https://doi.org/10.1107/s0021889801002242>
- Wang, F., Tange, Y., Irifune, T., & Funakoshi, K. I. (2012). P-V-T equation of state of stishovite up to mid-lower mantle conditions. *Journal of Geophysical Research*, 117(B6), B06209. <https://doi.org/10.1029/2011jb009100>
- Wang, S., Cai, N., Qi, X., Chen, S., & Li, B. (2021). Sound velocities of iron-nickel (Fe<sub>90</sub>Ni<sub>10</sub>) alloy up to 8 GPa and 773 K: The effect of nickel on the elastic properties of bcc-iron at high PT. *American Mineralogist: Journal of Earth and Planetary Materials*, 106(11), 1744–1750. <https://doi.org/10.2138/am-2021-7716>
- Wang, S., Chen, S., Qi, X., Xu, M., Yu, T., Wang, Y., & Li, B. (2024). Reassessment of Birch's Law on hcp-Fe from ultrasonic sound velocity measurement and implications on the velocity profiles of Earth's inner core. *Journal of Geophysical Research: Solid Earth*, 129(5), e2023JB027979. <https://doi.org/10.1029/2023jb027979>
- Weidner, D. J., Bass, J. D., Ringwood, A., & Sinclair, W. (1982). The single-crystal elastic moduli of stishovite. *Journal of Geophysical Research*, 87(B6), 4740–4746. <https://doi.org/10.1029/jb087ib06p04740>
- Williams, Q., & Revenaugh, J. (2005). Ancient subduction, mantle eclogite, and the 300 km seismic discontinuity. *Geology*, 33(1), 1–4. <https://doi.org/10.1130/g20968.1>
- Wölbern, I., & Rüpker, G. (2018). A sequence of up to 11 seismic discontinuities down to the midmantle beneath Southeast Asia. *Geochemistry, Geophysics, Geosystems*, 19(12), 4820–4835. <https://doi.org/10.1029/2018gc007827>
- Woodland, A. B. (1998). The orthorhombic to high-P monoclinic phase transition in Mg-Fe pyroxenes: Can it produce a seismic discontinuity? *Geophysical Research Letters*, 25(8), 1241–1244. <https://doi.org/10.1029/98gl00857>
- Xu, W., Lithgow-Bertelloni, C., Stixrude, L., & Ritsema, J. (2008). The effect of bulk composition and temperature on mantle seismic structure. *Earth and Planetary Science Letters*, 275(1–2), 70–79. <https://doi.org/10.1016/j.epsl.2008.08.012>
- Yamanaka, T., Fukuda, T., & Mimaki, J. (2002). Bonding character of SiO<sub>2</sub> stishovite under high pressures up to 30 GPa. *Physics and Chemistry of Minerals*, 29(9), 633–641. <https://doi.org/10.1007/s00269-002-0257-3>
- Yang, R., & Wu, Z. (2014). Elastic properties of stishovite and the CaCl<sub>2</sub>-type silica at the mantle temperature and pressure: An ab initio investigation. *Earth and Planetary Science Letters*, 404, 14–21. <https://doi.org/10.1016/j.epsl.2014.07.020>
- Zhang, Y., Fu, S., Karato, S. I., Okuchi, T., Chariton, S., Prakapenka, V. B., & Lin, J. F. (2022). Elasticity of hydrated Al-bearing stishovite and post-stishovite: Implications for understanding regional seismic VS anomalies along subducting slabs in the lower mantle. *Journal of Geophysical Research: Solid Earth*, 127(4), e2021JB023170. <https://doi.org/10.1029/2021jb023170>
- Zhang, Y., Fu, S., Wang, B., & Lin, J.-F. (2021). Elasticity of a pseudoproper ferroelastic transition from stishovite to post-stishovite at high pressure. *Physical Review Letters*, 126(2), 025701. <https://doi.org/10.1103/physrevlett.126.025701>